

Characterizations of BC501A and BC537 liquid scintillator detectors



Jianguo Qin^{a,b,c,*}, Caifeng Lai^b, Bangjiao Ye^a, Rong Liu^b, Xinwei Zhang^d, Li Jiang^b

^a Department of Modern Physics, University of Science and Technology of China, Hefei 230026, China

^b Institute of Nuclear Physics and Chemistry, China Academy of Engineering Physics, PO Box 213, Mianyang 621900, China

^c Graduate School, China Academy of Engineering Physics, Mianyang 621900, China

^d Institute of Applied Physics and Computational Mathematics, PO Box 8009, Beijing 100088, China

HIGHLIGHTS

- Light output resolution function of BC501A and BC537 detectors were derived.
- The γ -ray response matrices of two scintillator detector were simulated and validated.
- The γ -ray efficiency was simulated for four different energy thresholds below 7 MeV.
- A comparative study of detectors performance in different disciplines was performed.

ARTICLE INFO

Article history:

Received 8 February 2015

Received in revised form

16 May 2015

Accepted 4 June 2015

Available online 19 June 2015

Keywords:

Liquid scintillator detector

Light output function

Energy resolution function

γ -Ray response matrix

Detection efficiency

ABSTRACT

Two 2" \times 2" liquid scintillator detectors BC537 and BC501A have been characterized for their responses and efficiencies to γ -ray detection. Light output resolution and response functions were derived by least-squares minimization of a simulated response function, fitted to experimental data. The γ -ray response matrix and detection efficiency were simulated with Monte Carlo (MC) methods and validated. For photon energies below 2.4 MeV, the resolution, as well as the efficiency, of BC501A is better than BC537 scintillator. The situation is reversed when the energy is higher than 2.4 MeV. BC537 has higher γ -ray detection efficiency than BC501A if the impinging photon energy is more than 2 MeV due to different ratios of C to H/D atoms.

© 2015 Elsevier Ltd. All rights reserved.

1. Introduction

Neutron fields coexist with ambient γ -ray background with energies up to 10 MeV, produced mainly by the interaction of neutrons with structural materials of the experimental setup. Photon detectors should be insensitive to neutrons, or discriminate against neutron-induced events, e.g. by means of an appropriate threshold or pulse shape discrimination (PSD). For γ -ray dosimetry or spectroscopy, NaI (Tl), LaBr₃:Ce³⁺, BGO and HPGe detectors are often used if the neutron-induced events can be eliminated or corrected. However, the application of these photon spectrometers is limited in the case of mixed neutron/photon (n/ γ) fields. This is because appropriate experimental methods are not available, and the corrections for detector-related effects

("response matrices") are generally not known for these detectors. Additionally, for the HPGe detectors the neutron radiation damage is a serious issue prohibiting the extensive usage of the detectors in presence of strong neutron fields (Borrel et al., 1999), especially for the P-type Ge version.

Organic liquid scintillator detectors such as BC501A/NE213/EJ301 (molecular formula: C₆H₄(CH₃)₂, density: 0.874 g/cm³) offer excellent pulse shape discrimination abilities, which can be used to measure neutrons and photons in mixed n/ γ fields. Although these organic scintillators were originally specified for neutron spectrometry only (Mendell and Korff, 1963), some investigations have shown that these detectors are also well suited for photon spectrometry in a wide energy range (Goldberg et al., 1987; Yamamoto et al., 1989; Goldberg et al., 1990). BC537 (molecular formula: C₆D₆, density: 0.93 g/cm³) detectors are composed of deuteride benzene, also providing good PSD ability against n/ γ discrimination accompanied with low neutron sensitivity (Borella et al., 2007), and can be used to measure photons. The interaction of impinging photons to the scintillator material can be done

* Corresponding author at: Institute of Nuclear Physics and Chemistry, China Academy of Engineering Physics, PO Box 213, Mianyang 621900, China.

E-mail address: stingg@126.com (J. Qin).

through the photoelectric effect, Compton scattering and pair production (when $E_\gamma \gg 1.2$ MeV). For neutron detection, the dominant mechanism is the energy transfer of neutrons by scattering to hydrogen and deuterium atoms. The total neutron cross section ratio is about 1–1.5 for hydrogen to deuterium in the energy range 1–5 MeV, and it is 3–5 when the neutron energy is below 1 MeV. For the inelastic scattering of neutrons in the energy range of 5–20 MeV, the ratio of the total cross section varies between 1–1.25. As such, the BC537 detectors have much lower neutron detection efficiency, which changes with the neutron energy. Furthermore, the recoiling deuterium ions have a much lower energy than the recoiling protons for the same incident energy. This is because the deuterium mass is twice that of hydrogen, and this can lead to a lower neutron efficiency and light output for BC537 detectors. In contrast, BC537 detectors have advantages in measuring photons in n/γ mixed fields.

The responses of the incident particles on liquid scintillator detector are mainly determined as a function of the volume and shape of the liquid scintillator, and structure of the chamber. Reflector material and the photomultiplier tube (PMT) can also affect the response functions. The response matrix of the detector should be determined through a combination of experimental and Monte Carlo (MC) simulations.

The plan of the paper is as follows. The experimental setup for both detectors BC501A and BC537, as well as the electronic circuit, are described in Section 2. Four characteristic functions, including those for pulse shape, figure of merit (FoM), light output and resolution are introduced in Section 3. In Section 4, the measurements, the simulations and the spectra unfolding procedure are described. The conclusions of the present work are presented in Section 5.

2. Detector assembly and data acquisition

Two liquid scintillator detectors, BC537 and BC501A, were fabricated by Saint-Gobain for the studies described in this paper. Both detectors are 5.08 cm in diameter and length. The BC501A liquid scintillator (ratio of H:C atoms: 1.212) was coupled to a Photonics XP2020 PMT, with a high voltage of –1600 V applied. The BC537 liquid scintillator (ratio of H:C atoms: 0.99) was coupled to an Electron Tube 9807B photomultiplier tube, with a high

Table 1
Parameters of γ -ray sources.

Sources	E_γ /MeV	E_C /MeVee	Activity/kBq
^{241}Am	0.059	0.011	41.1
^{137}Cs	0.662	0.478	23.0
^{22}Na	1.274	1.062	19.0
^{54}Mn	0.511	0.341	35.4
	0.835	0.639	
^{58}Co	0.811	0.617	27.8
	0.898	0.699	
^{88}Y	1.836	1.612	22.5
^{24}Na	1.368	1.153	31.6
	2.754	2.52	
^{198}Au	0.412	0.254	19.7
^{51}Cr	0.321	0.179	16.8
$^{241}\text{Am-Be}$	4.43	4.198	1100

voltage of –1150 V applied. Both BC537 and BC501A detectors have the same number of electrons per cubic centimeter (www.detectors.saint-gobain.com). The scintillators of the BC537 and BC501A detectors are shown in Fig. 1. The detector volume of the BC501A is fully filled with liquid scintillator without any gas bubble, while the BC537 detector has a gas bubble. The liquid scintillator volume ratio ($V_{\text{BC537}}/V_{\text{BC501A}}$) is 0.895. Both of the detectors are placed horizontally in the experiments and simulations.

A number of calibrated γ -ray sources (point-like sources: ^{241}Am , ^{137}Cs , ^{22}Na , ^{54}Mn and ^{58}Co ; disk-like sources activated by neutrons: ^{88}Y , ^{24}Na , ^{198}Au and ^{51}Cr), as well as the $^{241}\text{Am-Be}$ neutron source (shown in Table 1), were used to determine the light output functions and the light resolution functions. $^{241}\text{Am-Be}$ neutron sources also emit γ -rays via the reaction $\text{Be}(\alpha, n)^{12}\text{mC}$, where the α particle is emitted from the decay of ^{241}Am . It will emit 4.43 MeV γ -rays when ^{12}mC decays from the excited state to the ground level. In order to obtain an approximately parallel γ -ray beam, a lead collimator with thickness of 5 cm and diameter of 2" was placed at the central axis between the source and the detector. The distance between the collimator and the detector is 5 cm, and the distance between the radioactive source and the front face of the detector is 15 cm. To measure the γ -rays in the mixed n/γ field of $^{241}\text{Am-Be}$, an electronic circuit (see Fig. 2) with a PSD function based on the zero-crossing method was used.

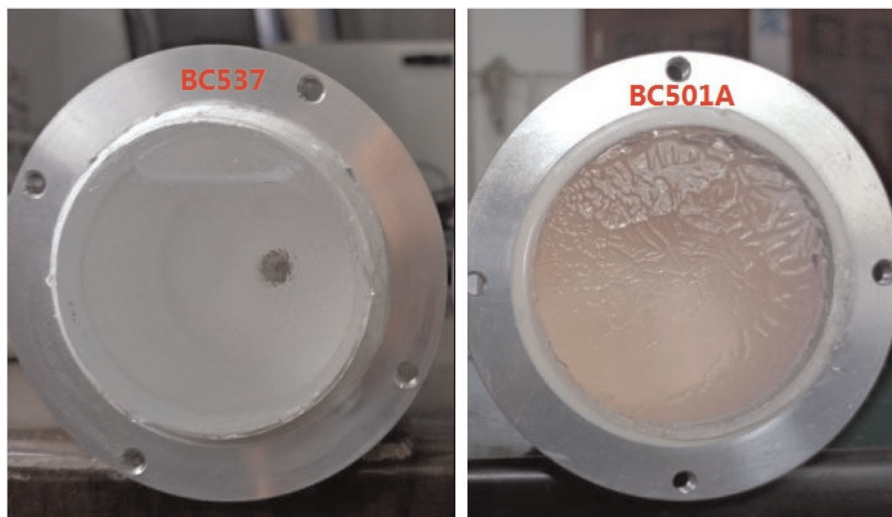


Fig. 1. Photos of BC537/BC501A liquid scintillators.

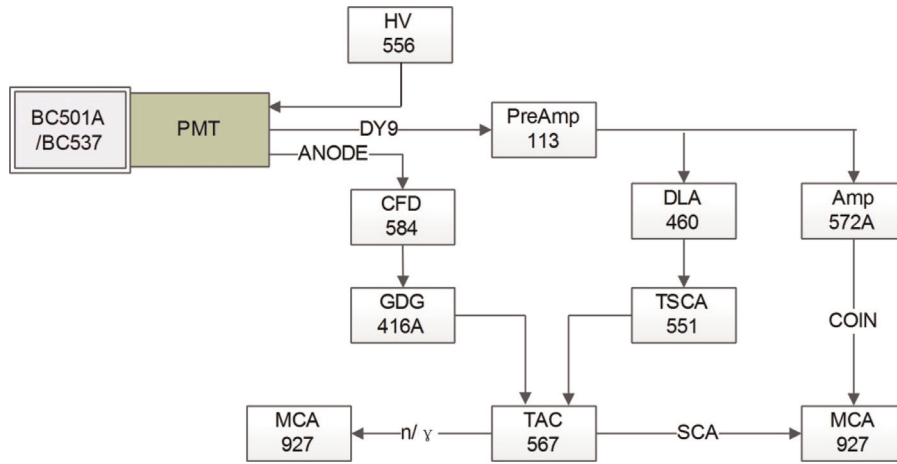


Fig. 2. Schematic of electronic circuit (all of the electronic modules are fabricated by ORTEC).

3. Characteristic functions

3.1. Pulse shape analysis and figure of merit

The shape and height of pulse are two dominant parameters to describe the resolutions of neutron and photon detection. Pulse shapes measured by the electronic circuit are a convolution of the exponential decay spectrum produced by the scintillator and the response functions of the photomultiplier and back-end electronics. An equation including three exponential functions can accurately model the pulse shape, as described by Eq. (1) (Marrone et al., 2002):

$$P_s = f_1(e^{-\theta(t-t_0)} - e^{-\lambda_s(t-t_0)}) + f_2(e^{-\theta(t-t_0)} - e^{-\lambda_l(t-t_0)}) \quad (1)$$

Where P_s is represent pulse shape, t_0 is reference time, θ , λ_s , and λ_l , are three exponential decay constants, f_1 and f_2 are normalization parameters. For a specific detector, different values of f_1/f_2 represent pulse shapes produced by different particles. Pulse shapes produced by Eq. (1) with different particles are shown in Fig. 3. NIM modules can be used to differentiate pulse shapes in the B-district, or the ratio of B-district to A-district, as shown in Fig. 3. The rise time, zero-crossing, and charge comparison methods are all considered.

Neutron and photon peaks can be always identified based on the n/γ discrimination spectrum. The FoM represents the resolution of

neutrons and photons, as defined in Eq. (2) (Yousefi et al., 2009):

$$\text{FoM} = D_{n\gamma}/(\text{FWHM}_\gamma + \text{FWHM}_n) \quad (2)$$

In the above equation, the terms FWHM_n and FWHM_γ correspond to the full width at half maximum of the distributions attributed to neutrons and γ -rays, respectively. $D_{n\gamma}$ refers to the distance between the two peaks. The measured neutron and γ -ray pulse shape spectrum of $^{241}\text{Am-Be}$ are shown in Fig. 4, which has a FoM of 1.5.

3.2. Light output functions

For modeling the scintillator detectors, determinations of the light output function $L(E)$ and the pulse height resolution function $dL/L(E)$ are of first important and strongly depends on the type of the interacting particle. The linear scale of the pulse height spectrum is usually calibrated in terms of electron energy if the photon energy lies in the energy range $40 \text{ keV} < E_\gamma < 1.6 \text{ MeV}$. The position of the Compton edge (P_C) and its equivalent electron energy (E_C) follow a linear relationship (Klein and Neumann, 2002):

$$P_C = G(E_C - E_0) \quad (3)$$

Where G is the calibration factor to convert the channel to the equivalent electron energy. The light output is $L_\gamma \propto (E_C - E_0)$, and the energy offset E_0 compensates for the non-linearity of the light

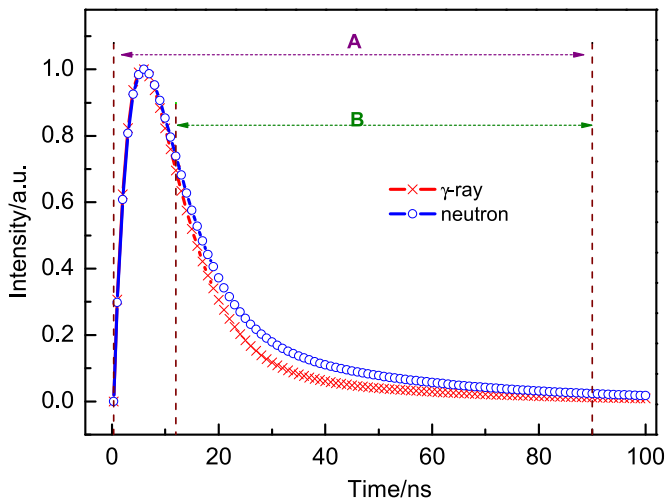


Fig. 3. n/γ pulse shape generated by Eq. (1).

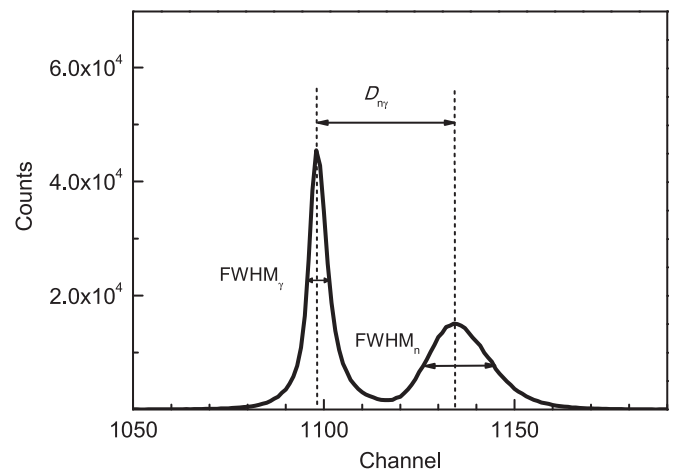


Fig. 4. n/γ discrimination of $^{241}\text{Am-Be}$ neutron source for the BC501A scintillator as resulted by implementing the zero-crossing method.

output due to quenching effects at low electron energies. For the proton, the relationship of light output L_p and energy E_p can be parameterized as $L_p = a_1 E - a_2(1 - \exp(-a_3 E^{a_4}))$ when the energy is in the range of 1 MeV < E_p < 300 MeV (Cecil et al., 1979). Eq. (3) can be approximated as $L_p = a_0 + a_1 E + a_2 E^2$ when the energy is in the range of 5 MeV < E_p < 17 MeV, where the parameters a_i ($i = 1$ to 4) are experimentally determined and depend on the type of recoil particle (Aksoy et al., 1994).

3.3. Light output resolution functions

The light output resolution function is given by Eq. (4) (Klein and Neumann, 2002):

$$\frac{dL}{L} = \sqrt{\alpha^2 + \frac{\beta^2}{L} + \frac{\gamma^2}{L^2}} \quad (4)$$

In Eq. (4) that the factor α corresponds to the position dependence of light transmission within the scintillator volume. The factor β represents the statistical variation of the photoelectron production mechanism and multiplication. The factor γ corresponds to the electronic noise of the detector signal, which can be ignored in practice.

A linear relationship can be determined between the light output L and the equivalent electron energy E , and thus the light output resolution function can be expressed as $\Delta E^2 = \alpha^2(E - E_0)^2 + (\beta/\lambda)^2(E - E_0) + (\gamma/\lambda)^2$. This can be simplified to $\Delta E^2 \approx \alpha^2 E^2 + (\beta/\lambda)^2 E + (\gamma/\lambda)^2$ when the photon energy is much greater than 5 keV. Eq. (5) is used to represent the energy resolution in the MCNP code (X-5 Monte Carlo Team, 2003):

$$\text{FWHM} = \Delta E = a + b\sqrt{E} + cE^2 \quad (5)$$

Eqs. (4) and (5) are not absolutely equivalent, so the parameters a , b and c cannot be expressed in terms of α , β and γ with analytical expressions, but there are approximate numerical results. For the same experimental data, similar results and two different parameter sets can be obtained through Eqs. (4) and (5), respectively.

The Gaussian distributions for the central energy E_0 can be given as $\rho = \frac{1}{\sqrt{2\pi}\sigma} \exp(-((kH - E_0)^2/2\sigma^2))$, where H is channel, k is the conversion coefficient between channel and equivalent electron energy, and E_0 is the energy of Compton edge. The relationship between the FWHM and σ is $\text{FWHM} = 2\sqrt{2 \ln 2} \sigma$ (Glimore, 2008). Thus, σ and E have a relationship as shown in Eq. (6):

$$\sigma = \frac{1}{2\sqrt{2 \ln 2}}(a + b\sqrt{E} + cE^2) \quad (6)$$

The comparison between the measured Compton spectrum $N_{\text{exp}}(H_i)$ and the simulated Compton spectrum $N_{\text{MC}}(H_i)$ depends on two parameters, the conversion factor G and the overall resolution σ of the scintillator-PMT and electronics chain. These parameters can be extracted from fitting to the spectrum measured experimentally. To evaluate the parameters G and σ , an iterative chi-squared minimization procedure is used, where χ^2 is defined in Eq. (7):

$$\chi^2 = \sum_i \frac{(N_{\text{exp}}(H_i) - N_{\text{MC}}(H_i))^2}{\sigma_{\text{exp}}^2(H_i)} \quad (7)$$

Where $N_{\text{exp}}(H_i)$ is the counts in the i th energy bin excluding the background of the experimental spectrum; $N_{\text{MC}}(H_i)$ is the corresponding spectrum simulated by MC; and $\sigma_{\text{exp}}(H_i)$ is the statistic error on the counts in the i th energy bin. After obtaining some groups of relationships (more than three) between the resolution σ_{E_i} and the energy E_i , the best fitting parameters a , b and c (or α , β

and γ) can be obtained with a Least-Squares-Fit of the entire experimental data. So, the light output resolution function and the energy resolution function can be expressed by the parameters accurately in the entire energy range.

4. Experimental measurement and simulation

4.1. Light output functions and γ -ray response

Light output functions of the BC501A and BC537 detectors were determined by using different γ -rays with energies up to 4.43 MeV. The resulting light output functions are shown in Figs. 5 and 6. The lines represent linear fits to the experimental data. For the BC501A/BC537 detectors, the energy offset (E_0) values are 3.58 keV and 2.0 keV, and the factors G are 233 channel/MeVee and 258 channel/MeVee, respectively.

The BC537 and BC501A liquid scintillators consist of carbon, hydrogen and deuterium that have low atomic numbers (Z). High energy photons cannot entirely deposit their energy since the photoelectric cross section is proportional to Z^5 . Therefore, in the measured spectra by these liquid scintillator detectors, the full energy photo peak is not formed. Accordingly, the recoil electron spectrum has to be used to reconstruct the energy of the detected photons.

γ -Ray response functions of BC501A and BC537 have been measured for 13 γ -rays emitted by ten radio sources listed in Table 1, where energies of all γ -rays are in the range of 59.6 keV to 4.43 MeV. The measured recoil electron spectrum is broader than the simulated spectrum due to noise and statistic fluctuations. To account for these effects, the method introduced in Section 3.3 was used to broaden the simulated spectrum to match the measured spectrum. Some representative spectra of BC537 are shown in Fig. 7.

The full energy peak for 59.6 keV γ -ray can be measured if the gain is amplified by a factor of 10, as shown in Fig. 7(a). The experimental data are fitted with a Gaussian distribution function, where the central position of the peak represents the γ -ray energy, while the FWHM of the peak represents the energy resolution. The experimental and simulated spectra of 662 keV photons emitted by a ^{137}Cs radionuclide source are shown in Fig. 7(b). L_{max} and L_C are positions of the maximum probability and the Compton edge, while $L_{1/2}$ is the location of half-maximum intensity. The simulation agrees well with the experiment above 0.2 MeVee, the

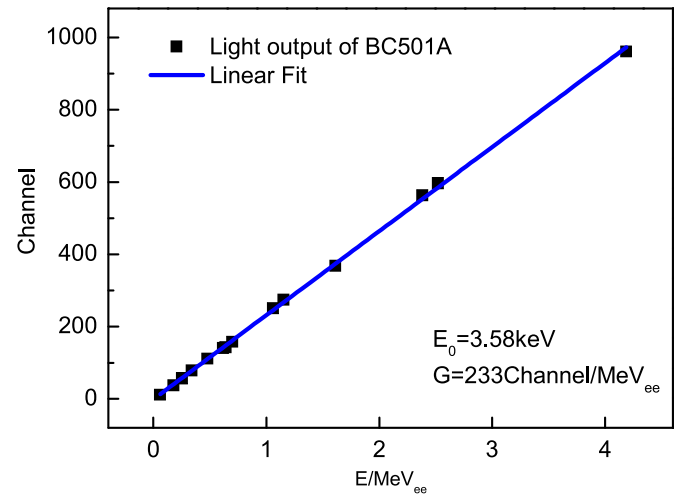


Fig. 5. Light output of BC501A generated by γ -rays.

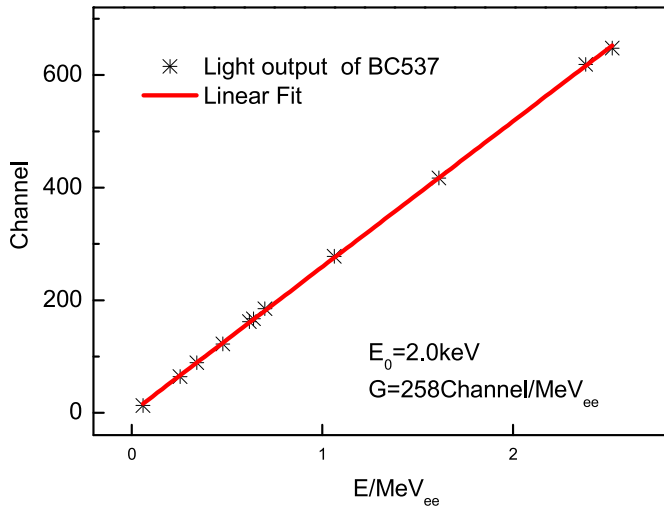


Fig. 6. Light output of BC537 produced by γ -rays.

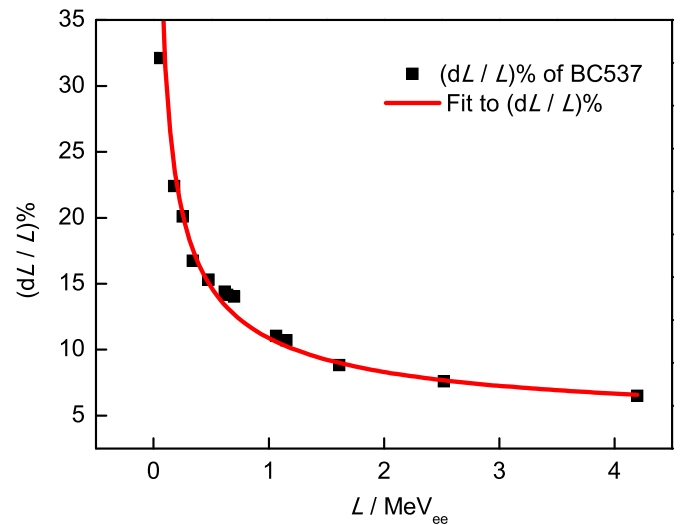


Fig. 8. Light output resolution function of BC537.

discrepancy below 0.2 MeVee is due to the contribution of scatter of the experimental data. Results from 2.75 MeV and 4.43 MeV γ -rays are shown in Fig. 7(c) and (d), respectively. The model also agrees well with the observation in the energy range $E_{SE} < E < L_{1/2}$, where E_{SE} represents the peak energy of the single escaping electron pair. The discrepancy beyond the location of $L_{1/2}$ is due to the summing effect of the recoil electron and the second recoil

electron that were generated by the scattered γ -rays.

4.2. Energy resolution and the Compton edge

The recoil electron energy is maximal when back scattering occurs, and can be expressed by $E_{max} = E_\gamma^2 / ((m_0 c^2 / 2E_\gamma) + 1)$. This

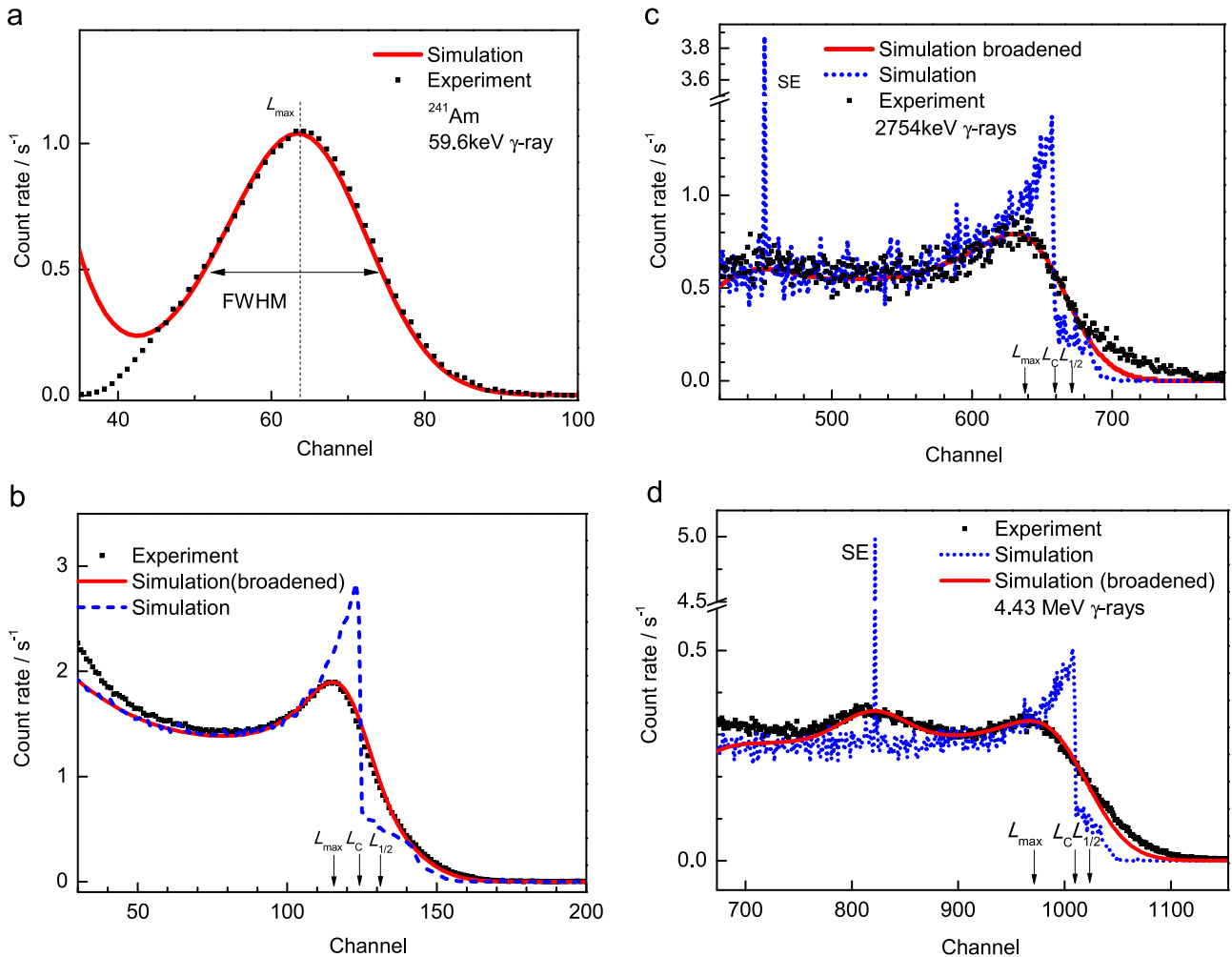


Fig. 7. Four experimental and simulated electron recoil spectra of BC537. (a) 59.6 keV, (b) 662 keV, (c) 2754 keV, and (d) 4.43 MeV.

corresponds to the Compton edge energy. The energy calibration needs to confirm the exact Compton edge in the recoil electron spectrum. Generally, MC (The ICARUS Collaboration, 1998; Matei et al., 2012) and γ - γ coincidence methods (Smith et al., 1968; Konx and Miller, 1972; Jie et al., 2010) are used to identify the Compton edge. The recoil electron spectrum has a roughly Gaussian shape and can be obtained using the γ - γ coincidence method, but it requires photons with high energy and high intensity. Therefore, MC methods are more commonly used to predict the Compton edge and energy resolution.

The energy resolutions and Compton edges of BC537 and BC501A were obtained according to the experimental data for 13 γ -rays listed in Table 1 and compared with the corresponding Monte Carlo calculations performed within the present work. The measured light output resolution function for BC537 is shown in Fig. 8, where the curve represents the best fitting to Eq. (4). The values of the parameters α , β and γ are 3.13%, 9.926% and 8.06×10^{-6} %, respectively. The primary influence factor β agrees with the previous results of the BC501A detector ($\beta=10.2\%$, (The ICARUS Collaboration, 1998); $\beta=10.3\%$, (Jie et al., 2010)). The energy resolution function of BC537 is shown in Fig. 9, where the fitted curve represents the best fitting to Eq. (5) with parameter a , b and c are -0.008 , 0.117 and 0.083 , respectively. Fig. 10 shows the intensity ratio of L_C to L_{\max} , for BC537, which is (0.75 ± 0.02) and

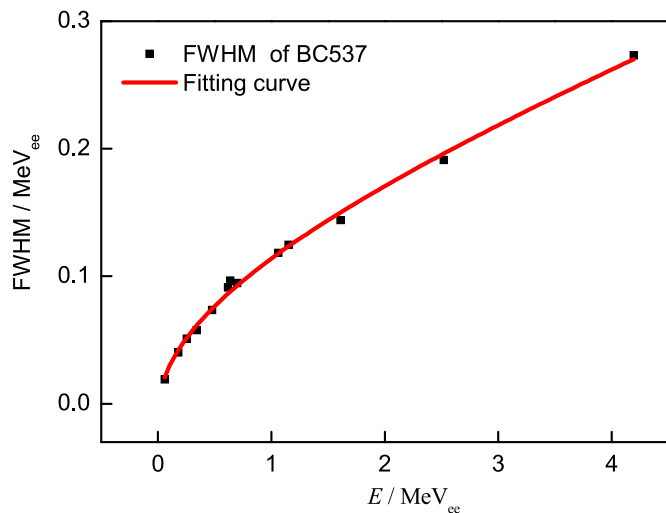


Fig. 9. Energy resolution function of BC537.

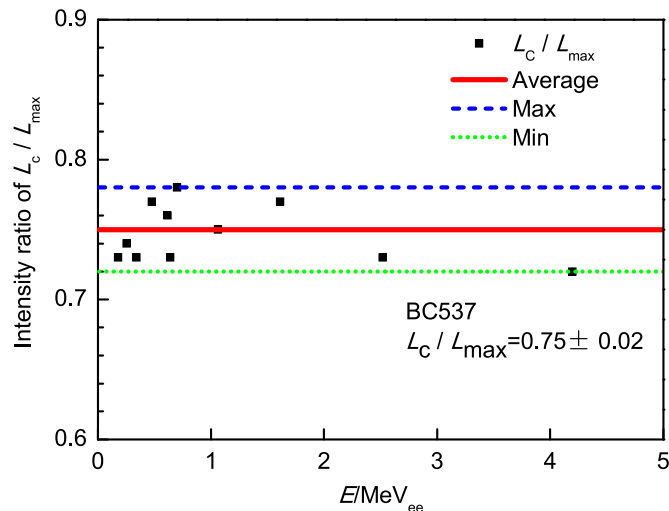


Fig. 10. Ratios of L_C/L_{\max} for BC537.

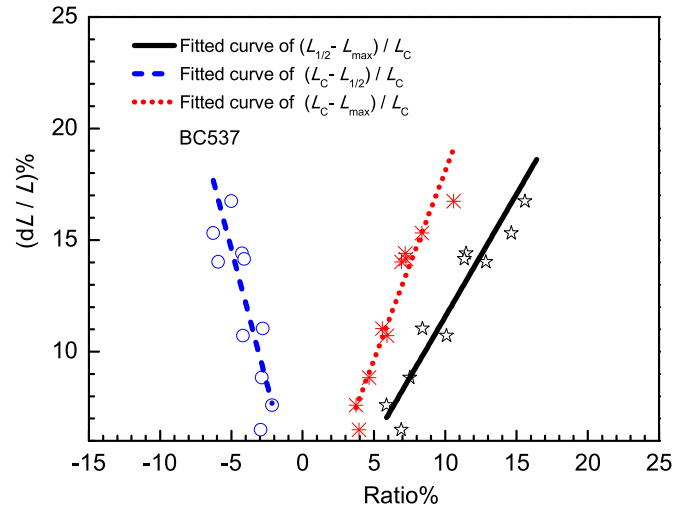


Fig. 11. Light output resolution of BC537 vs. ratios of $(L_C - L_{\max})/L_C$, $(L_C - L_{1/2})/L_C$, and $(L_{1/2} - L_{\max})/L_C$.

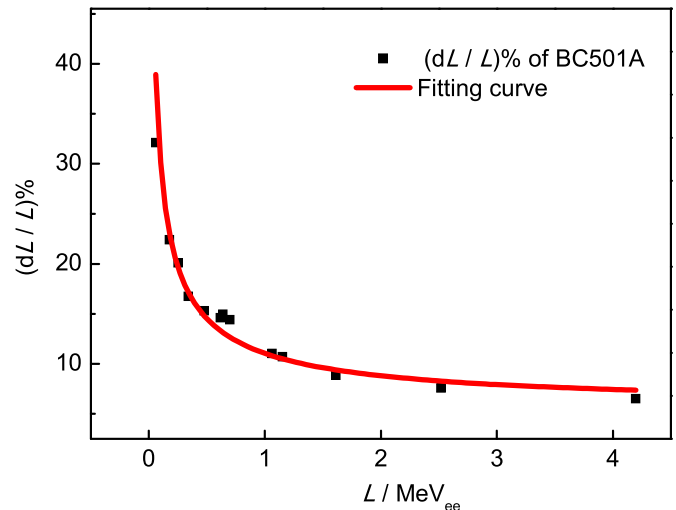


Fig. 12. Light output resolution function of BC501A.

closed to the results of NE213 (equal to BC501A) reported by Dietze and Klein (1982). The relationship of the light output resolution and the ratios of $(L_C - L_{\max})/L_C$, $(L_C - L_{1/2})/L_C$ and $(L_{1/2} - L_{\max})/L_C$ are shown in Fig. 11.

For the BC501A liquid scintillator detector, the light output resolution function and energy resolution function are shown in Fig. 12 ($\alpha=5.96\%$, $\beta=7.65\%$, $\gamma=0.49\%$) and Fig. 13 and 14 ($a=-0.001$, $b=0.078$, $c=0.608$), respectively. The relationship between the light output resolution and the ratios of $(L_C - L_{\max})/L_C$, $(L_C - L_{1/2})/L_C$ and $(L_{1/2} - L_{\max})/L_C$ are shown in Fig. 15. These results are roughly consistent with those of the BC537 detector. The comparison of the fitted light output resolution functions below 7 MeVee is shown in Fig. 16. The resolution of the BC501A detector is better than that of the BC537 detector for energy below 2.4 MeVee, and the results are reversed when the energy is above 2.4 MeVee. Fig. 14 shows the ratio of L_C to L_{\max} for BC501A, which is (0.76 ± 0.04) and is closed to the results of BC537.

Energy calibration results of L_C , L_{\max} and $L_{\max}/2$ for the BC501A detector are shown in Fig. 17. The results calibrated by L_C show that the offset is 3.85 keV and the factor G has an uncertainty of 0.7%, which is similar to the results of Klein and Neumann (2002). For the position of L_{\max} is not easily recognizable, the results

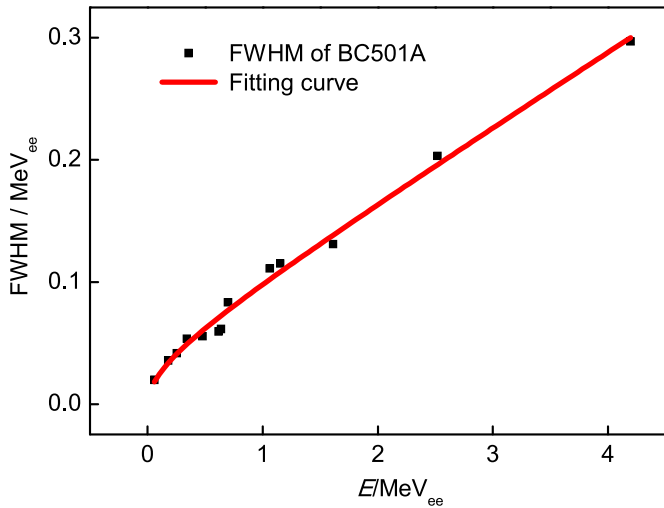


Fig. 13. Energy resolution function of BC501A.

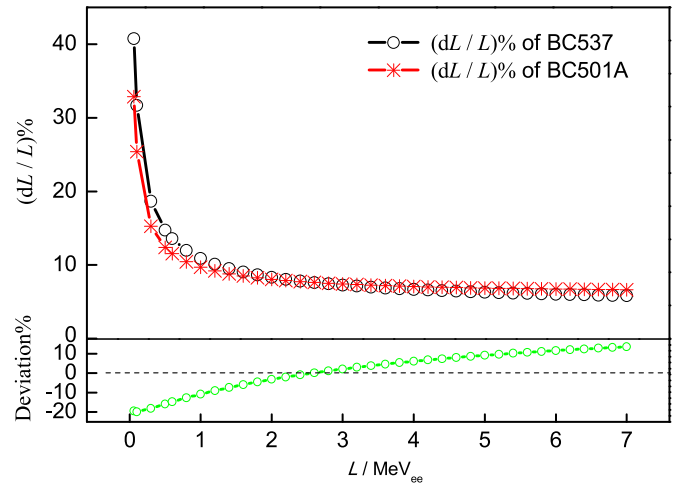


Fig. 16. Light output resolution of BC537 and BC501A.

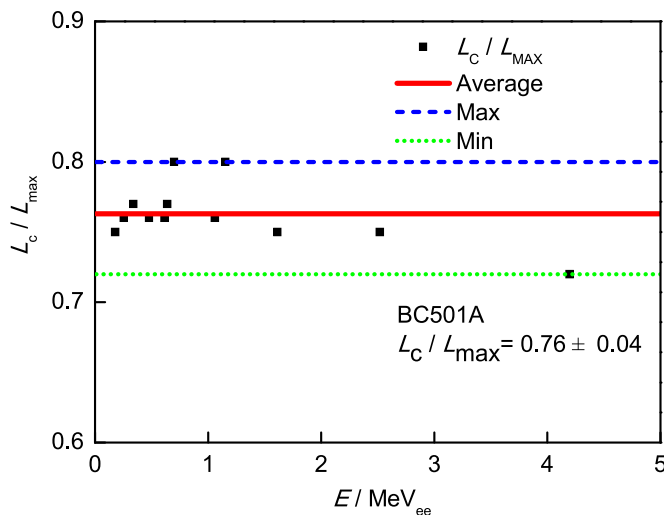


Fig. 14. Ratios of L_c/L_{max} for BC501A.

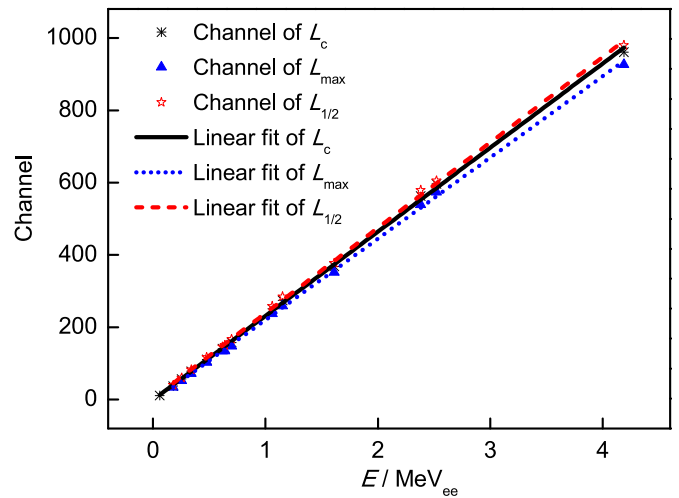


Fig. 17. Energy calibration for BC501A with L_c , L_{max} , and $L_{1/2}$, respectively.

calibrated by L_{max} show an offset of 19.4 keV and have a relative deviation of 3.6% with respect to the results calibrated by L_c .

4.3. Simulation of response matrix

Detector response functions for BC537 and BC501A were simulated using MCNP code, corresponding to a beam of incident

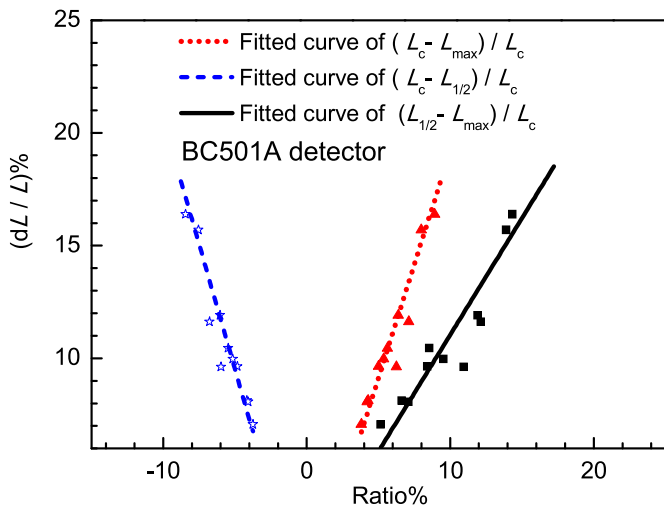


Fig. 15. Light output resolution of BC501A vs. $(L_c - L_{max})/L_c$, $(L_c - L_{1/2})/L_c$, and $(L_{1/2} - L_{max})/L_c$.

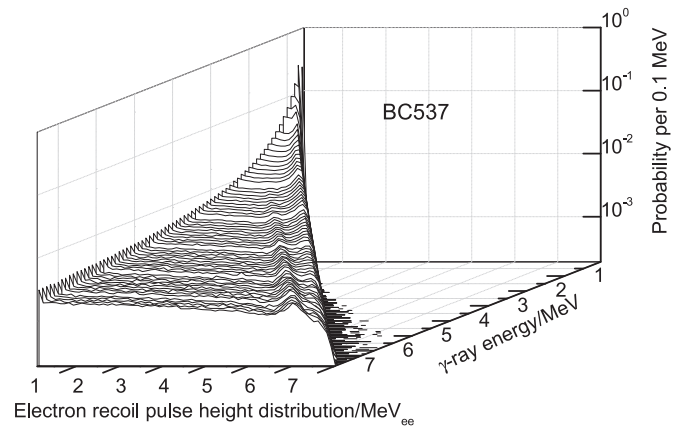


Fig. 18. γ -Ray response matrix of BC537.

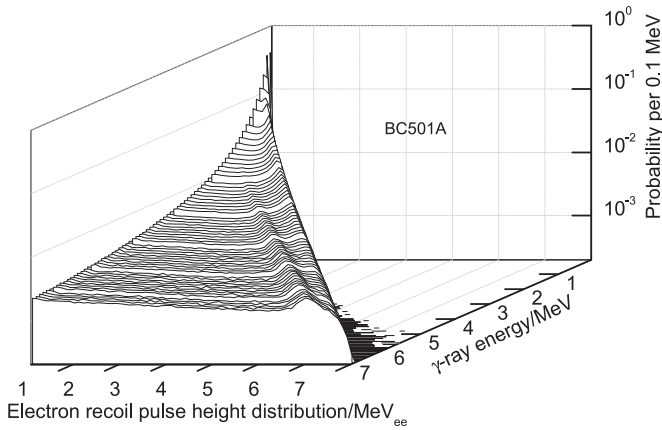


Fig. 19. γ -Ray response matrix of BC501A.

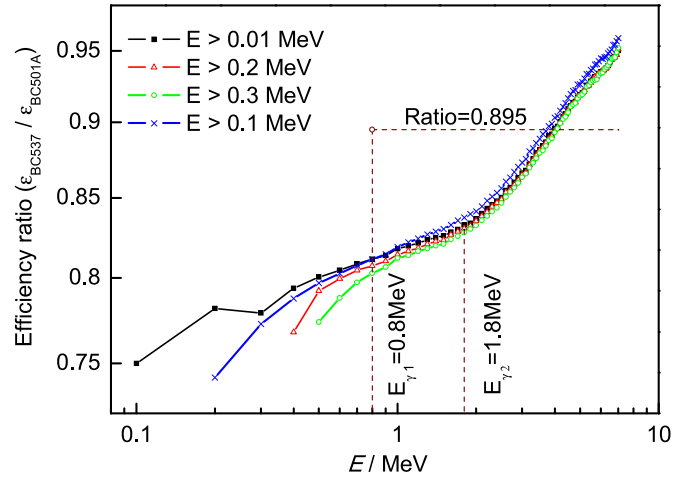


Fig. 21. Efficiency ratio of BC537 to BC501A.

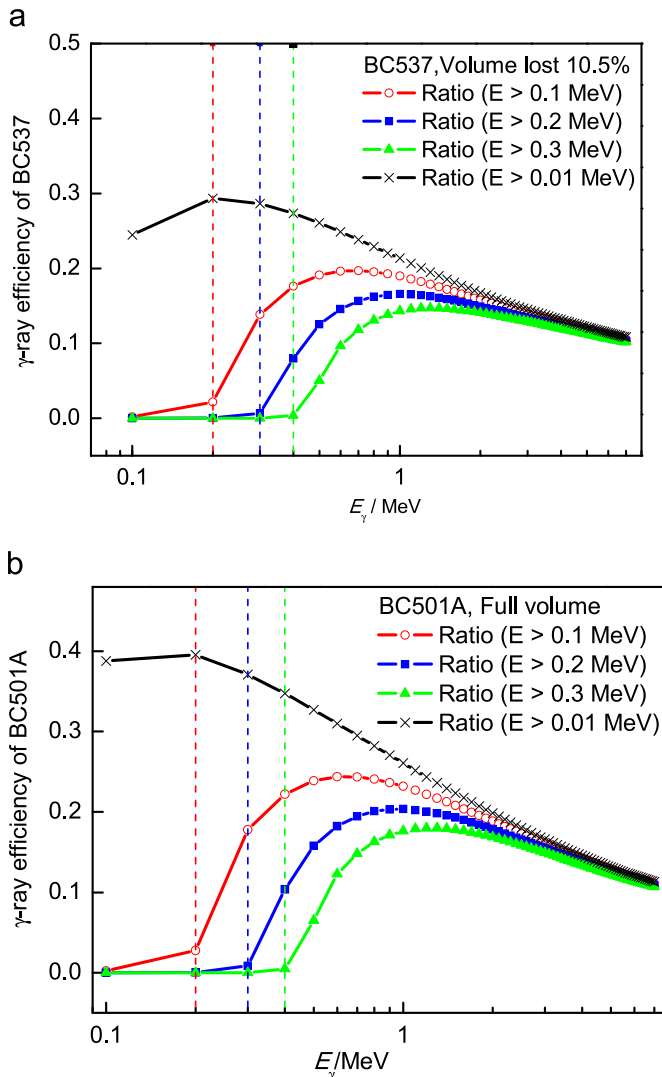


Fig. 20. Efficiency curve for different energy threshold. (a) BC537, (b) BC501A.

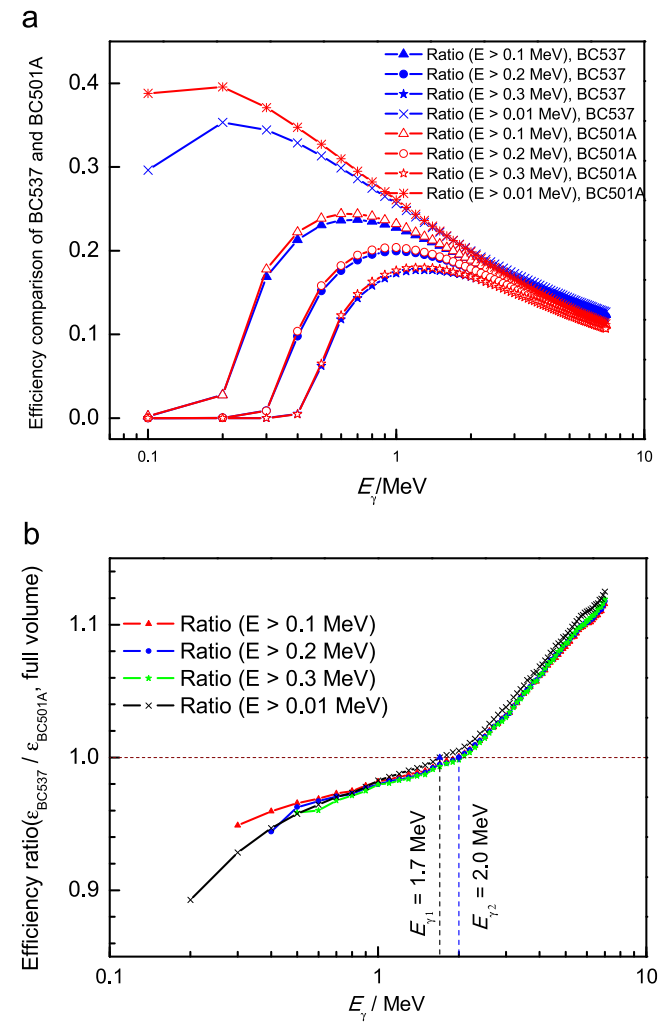


Fig. 22. Efficiency comparison of BC537 and BC501A with full volume. (a) Efficiency of BC501A and BC537, (b) efficiency ratio of BC537 to BC501A.

parallel γ -rays with a radius of 2.54 cm. To include the broadening factors described above, the parameters a , b and c described in Section 4.1 are used as input to the MC. Finally, we obtain the response matrix with 70×70 bins below 7 MeV, with a bin width of 0.1 MeV. The response matrices are shown in Figs. 18 and 19, where axes of X , Z and Y represent energy of the recoil electrons, normalized intensity and the energy of the γ -rays, respectively.

4.4. Photon efficiency simulation

The efficiencies of the BC537 and BC501A detectors for various energy thresholds were simulated by MCNP to investigate the influence of liquid scintillator volume on the γ -ray detection

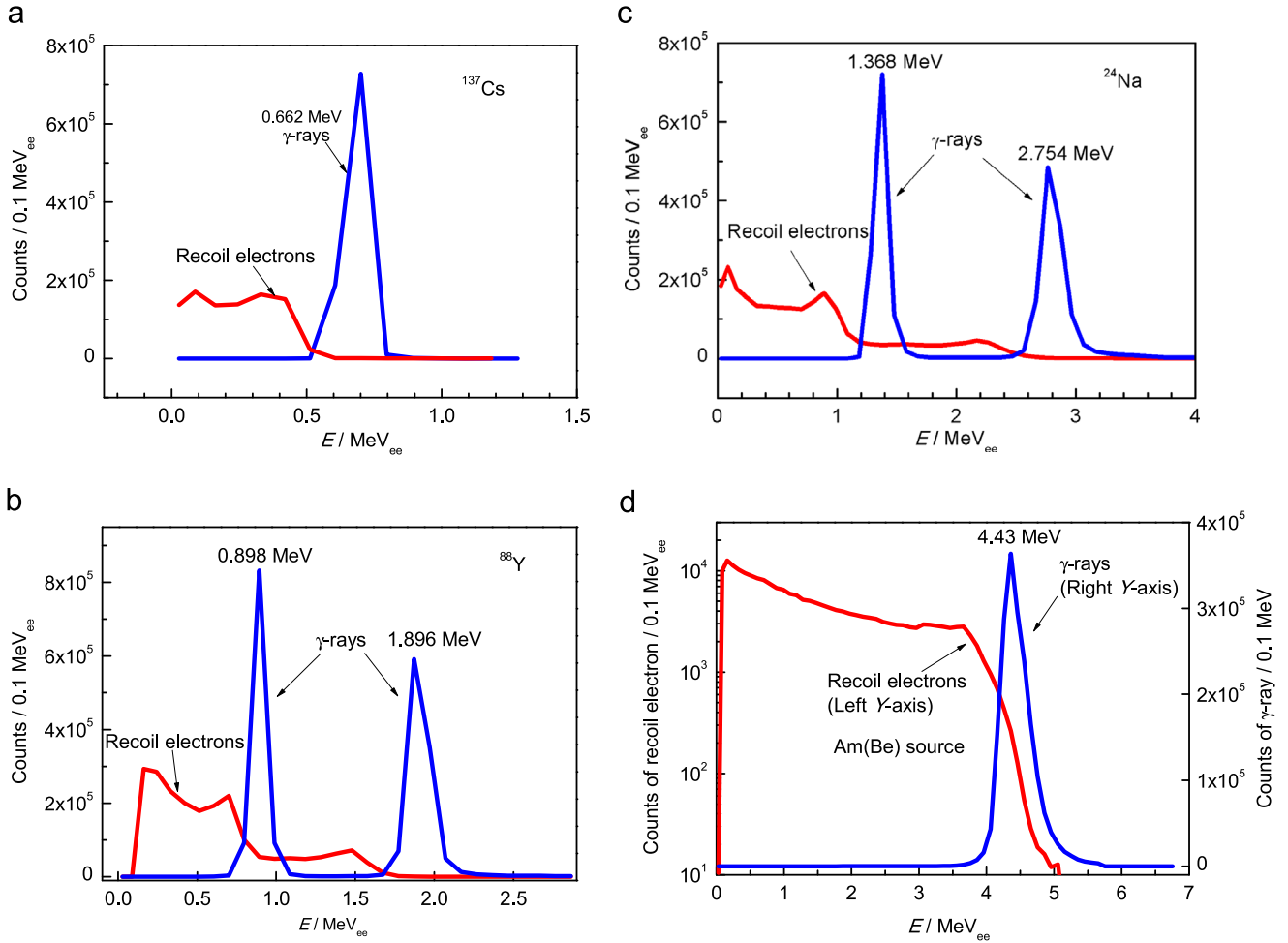


Fig. 23. Recoil electron spectra and the γ -ray spectra unfolded using the GRAVEL method. (a) ^{137}Cs , (b) ^{88}Y , (c) ^{24}Na , and (d) ^{241}Am -Be neutron source.

efficiency. The efficiency curves of the BC537 and BC501A detectors with four different energy thresholds are shown in Fig. 20. They are roughly consistent with each other. A relative comparison of the BC537 and BC501A detectors is shown in Fig. 21, where the horizontal dotted line represents a liquid scintillator volume ratio ($V_{\text{BC537}}/V_{\text{BC501A}}$) of 0.895. The efficiency deviation varies with energy threshold for energies below 0.8 MeV, but the efficiencies approach to a number for energies above 0.8 MeV. The ratio varies from 80% to 95% when the energy rises from 0.8 MeV to 7 MeV.

The simulated efficiencies of photons induced in BC537 and BC501A detectors with energies below 7 MeV are shown in Fig. 22 (a). The BC501A detector has a higher efficiency if the photon energy is below 2 MeV. Fig. 22(b) shows the deviation more clearly. The four efficiency ratio curves are agree well with each other for the energy range 1.7–2 MeV. But BC537 has a higher efficiency than BC501A if the photon energy is above 2 MeV, where there is a $\sim 12\%$ deviation at 7 MeV. For the high-energy photons, pair production is the main production mode. The pair production cross section σ_p is proportional to the square of the atomic number Z and the induced γ -ray energy E_γ ($\sigma_p \propto Z^2 E_\gamma$; or $\sigma_p \propto Z^2 \ln E_\gamma$, if $E_\gamma \gg m_0 c^2$, m_0 is electron rest mass). Since BC537 has a higher atom ratio (C:D) than BC501A (C:H), the BC537 liquid scintillator would have a higher effective atomic number Z_{eff} , which results in a higher pair production cross section than BC501A for the high-energy impinging γ -rays.

4.5. Recoil electron spectrum unfolding

4.5.1. Principles of unfolding procedure

The relationship between the recoil spectrum and the γ -ray spectrum could be expressed as $\Phi_e(E) = \int M(H, E) \Phi_\gamma(E) dE$. It also could be transformed to a matrix equation $\Phi_e(E) = M(H, E) \Phi_\gamma(E)$, where $\Phi_e(E)$ is the recoil electron spectrum, $M(H, E)$ is the γ -ray response matrix, and $\Phi_\gamma(E)$ is the γ -ray spectrum (Matzke, 2002). Generally, there are many unfolding methods such as the matrix inversion method, the least squares method (Stalman, 1986), the neural network method (Sharghi Ido et al., 2009; Ortiz-Rodríguez et al., 2014), and GRAVEL methods (Chen et al., 2014), etc. The GRAVEL iterative method was chosen to unfold the recoil electron spectra in this paper.

GRAVEL is a modified version of the SAND-II method (McElory et al., 1967). Given a discrete spectrum f_i^j , it defines the next iteration according to the Eq. (8) (Reginatto, 2003):

$$f_i^{j+1} = f_i^j \exp \left[\frac{\sum_k W_{ik}^j \log \left[\frac{N_k}{\sum_i R_{ki} f_i^j} \right]}{\sum_k W_{ik}^j} \right] \quad (8)$$

where, N_k is the number of events in the k th bin of the measured spectrum, σ_k is the estimate of the measurement uncertainty, R_{ki} is the response matrix, and

$W_{ik}^j = (R_{ki}f_i^j / \sum R_{ki}f_i^j)(N_k^2/\sigma_k^2)$. The default spectrum f_i^j is used for the first iteration. This iterative procedure always leads to a non-negative spectrum that has a lowest χ^2 value.

4.5.2. Unfolded spectra

Electron recoil spectra measured by the BC501A and BC537 detectors were unfolded based on the GRAVEL method with response matrices as described in Section 4.3. The spectra considered include the γ -rays emitted by ^{137}Cs , ^{24}Na , ^{88}Y and ^{241}Am -Be radio sources. Electron recoil spectra measured by the BC501A detector and the corresponding γ -ray spectra are shown in Fig. 23.

The agreement between the unfolded and expected γ -ray spectra is good when the statistic uncertainty of the recoil electron spectrum is sufficient. The energy resolutions for the 0.662 MeV, 1.368 MeV and 4.43 MeV sources are 19.9%, 14.7% and 7.9%, respectively. The FWHM for 0.662 MeV photons is 0.13 MeV, which is wider than that of the energy bin (0.1 MeV). Based on the resolutions of the BC537 and BC501A detectors, the 0.1 MeV energy bin is reasonable when the energies of the induced γ -rays are less than 7 MeV.

5. Conclusions

In this work, the characterizations of BC537 and BC501A liquid scintillators with dimensions of $2'' \times 2''$ are presented. The detectors were characterized for their responses and efficiencies to detect γ -rays using calibrated radionuclide γ -ray sources in the energy range from 59.6 keV to 4.43 MeV. The ratios of L_C to L_{\max} for the two detectors were determined by Monte Carlo computation, and were determined to be (0.75 ± 0.02) and (0.76 ± 0.04) for the BC537 and BC501A detectors, respectively. Light output resolution functions and energy resolution functions of the two detectors were obtained using a least squares adjustment to experimental data using the simulated response. The results show that the resolution of BC501A is better than BC537 if the energy is below 2.4 MeV, but the results are reversed if the energy is above 2.4 MeV. The detector response matrices for γ -rays were derived, and validated by unfolding the γ -ray spectra using the GRAVEL iterative method.

We have simulated the γ -ray detection efficiency at four energy thresholds. For the same liquid scintillator with dimensions of $2'' \times 2''$, the BC501A detector has higher efficiency when the photon energy is below 2 MeV. For higher photon energies, the BC537 detector has higher efficiency, with a discrepancy of $\sim 12\%$ at 7 MeV.

The results presented in this work indicate that the BC501A and BC537 detectors are suitable for use in mixed n/γ fields, with an energy range from tens of thousands of electron volts to a few mega electron volts. It also provides a reference for readers in selecting appropriate detector and calculating γ -ray response matrix using the energy resolution parameters.

Acknowledgments

This work was supported by the National Natural Science Foundation of China (91226140). We would like to thank Mou Yunfeng and Wang Mei for their helpful experimental operation and discussions. We also thank Zhang Wushou, Hu Biao, Ma Yue and Lin Dexu for their valuable language comments and discussions. We are indebted to the reviewers of this paper for their constructive remarks.

References

- Aksoy, A., Coban, A., Naqvi, A.A., Khiari, F.Z., Hanly, J.M., Howell, C.R., Tornow, W., Felsher, P.D., Al-Ohali, M.A., Walter, R.L., 1994. Response-function measurement of an NE213 scintillator using the $^2\text{H}(d,n)^3\text{He}$ reaction. Nucl. Instrum. Methods Phys. Res. Sect. A 337, 486–491.
- Borrel, V., Kandel, B., Albernhe, F., Frabel, P., Cordier, B., Tausin, G., Crespin, S., Coszach, R., Denis, J.M., Leleux, P., 1999. Fast neutron-induced damage in IN-TEGRAL n-type HPGe detectors. Nucl. Instrum. Methods Phys. Res. Sect. A 430, 348–362.
- Borella, A., Aerts, G., Gensing, F., Moxon, M., Schilebeeckx, P., Wynants, R., 2007. The use of C_6D_6 detectors for neutron induced capture cross-section measurements in the resonance region. Nucl. Instrum. Methods Phys. Res. Sect. A 577, 626–640.
- Cecil, R.A., Anderson, B.D., Madey, R., 1979. Improved predictions of neutron detection efficiency for hydrocarbon scintillators from 1 MeV to about 300 MeV. Nucl. Instrum. Methods 161, 439–447.
- Chen, Y., Chen, X., Lei, J., An, L., Zhang, X., Shao, J., Zheng, P., Wang, X., 2014. Unfolding the fast neutron spectra of a BC501A liquid scintillation detector using GRAVEL method. Sci. China Phys. Mech. Astron. 57, 1885–1890.
- Dietze, G., Klein, H., 1982. Gamma-calibration of NE213 scintillation counters. Nucl. Instrum. Methods Phys. Res. 193, 549–556.
- Goldberg, E., Hansen, L.F., Howerton, R.J., Komoto, T.T., Poul, B.A., 1987. Gamma-Ray Emission from Spheres Pulsed with D-T neutrons: Results of May 1987 Experiments at TRNS-1. Report: UCID-21276. USA.
- Goldberg, E., Hansen, L.F., Komoto, T.T., Pohl, B.A., Howerton, R.J., Dye, R.E., Plechaty, E.F., Warren, W.E., 1990. Neutron and gamma-ray spectra from a variety of materials bombarded with 14 MeV neutrons. Nucl. Sci. Eng. 105, 319–340.
- Glimore, Gordon R., 2008. Practical Gamma-Ray Spectrometry, 2nd Ed. Nuclear Training Services Ltd., Warrington, UK.
- Jie, Y., Rong, L., Cheng, L., Li, J., Xinxin, L., Tonghua, Z., 2010. Energy calibration of a BC501A liquid scintillator using a γ - γ coincidence technique. Chin. Phys. C 34, 993–997.
- Klein, H., Neumann, S., 2002. Neutron and photon spectrometry with liquid scintillation detectors in mixed fields. Nucl. Instrum. Methods Phys. Res. A 476, 132–142.
- Konx, H.H., Miller, T.G., 1972. A technique for determining bias settings for organic scintillators. Nucl. Instrum. Methods 101, 519–525.
- Marrone, S., Cano-Ott, D., Colonna, N., Domingo, C., Gramagna, F., Gonzalez, E.M., Gensing, F., Heil, M., Kappeler, F., Mastinu, P.F., Milazzo, P.M., Papaevangelou, T., Pavlopoulos, P., Plag, R., Reifarh, R., Tagliente, G., Tain, J.L., Wisshak, K., 2002. Pulse shape analysis of liquid scintillator for neutron studies. Nucl. Instrum. Methods Phys. Res. Sect. A 490, 299–307.
- Marcel Reginatto, 2003. The "Multi-Channel" Unfolding Programs in the UMG Package: MXD_MC32 and IQU_MC32, and GRV_MC32 (Version 3.2). PTB, Germany.
- Matei, C., Hamsch, F.-J., Oberstedt, S., 2012. Proton light output function and neutron efficiency of a p-terphenyl detector using a ^{252}Cf source. Nucl. Instrum. Methods Phys. Res. Sect. A 676, 135–139.
- Matzke, M., 2002. Propagation of uncertainties in unfolding procedures. Nucl. Instrum. Methods Phys. Res. Sect. A 476, 230–241.
- McElory, W.N., Berg, S., Crockett, T., Hawkins, R.G., 1967. SAND II (Report AFWL-TR-67-41). US Weapons Laboratory, United States.
- Mendell, R.B., Korff, S.A., 1963. Fast-Neutron Detector with Discrimination against Background Radiation. Rev. Sci. Instrum. 34 (12), 1356–1360.
- Ortiz-Rodríguez, J.M., Reyes Alfaro, A., Reyes Haro, A., Cervantes Viramontes, J.M., Vega-Carrillo, H.R., 2014. A neutron spectrum unfolding computer code based on artificial neural networks. Radiat. Phys. Chem. 95, 428–431.
- Stalman, F.W., 1986. LSL-M2: a Computer Program for Least-squares Logarithmic Adjustment of Neutron Spectra. Report: ORNL/TM-9933.
- Smith, D.L., Polk, R.G., Miller, T.G., 1968. Measurement of the response of several organic scintillators to electrons, protons and deuterons. Nucl. Instrum. Methods 64, 157–166.
- Sharghi Ido, A., Bonyadi, M.R., Etaati, G.R., Shahriari, M., 2009. Unfolding the neutron spectrum of a NE213 scintillator using artificial neural networks. Appl. Radiat. Isot. 67, 1912–1918.
- The ICARUS Collaboration, 1998. Calibration of BC501A liquid scintillator cells with monochromatic neutron beams. Nucl. Instrum. Methods Phys. Res. Sect. A 418, 285–299.
- X-5 Monte Carlo Team, 2003. MCNP-A General Monte Carlo N-Particle Transport Code, Version 5. Volume II: User's Guide.
- Yamamoto, J., Kanaoka, T., Murata, I., Takahashi, A., Sumita, K., 1989. Gamma-Ray Emission Spectra from Spheres with 14-MeV Neutron Source. Report: JAERI-M89-026. Japan.
- Yousefi, S., Lucchese, L., Aspinall, M.D., 2009. Digital discrimination of neutrons and gamma-rays in liquid scintillators using wavelets. Nucl. Instrum. Methods Phys. Res. Sect. A 598, 551–555.